Cluster- and energy-separated extreme states in a synthesized superatomic solid

Chaoyu Li,[1] Shengru Han,[1] Zhifeng Liu ●,[1,*] and Jijun Zhao[2,†]

[1]*School of Physical Science and Technology, Inner Mongolia University, Hohhot 010021, China*
[2]*Key Laboratory of Materials Modification by Laser, Ion and Electron Beams*
(Dalian University of Technology), Ministry of Education, Dalian 116024, China

Compared with conventional atomic crystals, superatomic solids are more attractive for providing opportunities to generate unexpected emergent states associated with their unique hierarchical structure. Using first-principles calculations, herein, we identify two cluster- and energy-separated extreme states in a synthesized binary fulleride. An emergent superatomic Dirac state and a flat band with extreme effective mass are found on different sides of the Fermi level, which are separately contributed by different constituent clusters. The coexistence of Dirac and flat states in a semiconductor rather than a metal/semimetal may open a door for constructing Dirac field-effect devices, giving rise to ultrafast Dirac carrier transport.

I. INTRODUCTION

In Dalton's atomic theory, atoms are the building blocks of matter. As the bridge between individual atoms and bulk solids, clusters are often referred to as *superatoms* [1–8] since some special clusters with atomically precise size and composition can mimic the behavior of an individual atom on the periodic table. Moreover, adding or subtracting one atom or even one electron in a cluster may cause notable changes in its structure and properties, thereby opening up endless possibilities. Bearing this in mind, numerous efforts were devoted to exploring a class of materials, i.e., cluster-assembled or superatomic crystalline materials [9–15], by taking superatoms instead of atoms as building blocks.

Compared with atomic crystals, superatomic crystals have the following two distinctive features [8,9]. Firstly, the *building blocks* of superatomic crystals are more diverse due to the fact that the properties of superatoms depend on some additional degrees of freedom, such as the cluster size and geometry; thus, the diversity of superatoms endows the cluster-assembled crystals with interesting degrees of freedom and tunability of material properties. Secondly, superatomic materials have unique hierarchical structures at two levels: the internal structure of the building clusters determined by interatomic interaction in a small length scale and the periodic lattice pattern formed by intercluster interaction in a large scale. Therefore, superatom- or cluster-assembling becomes an attractive approach to design functional materials with tailored properties, such as semiconductivity with tunable electronic properties [12,16–18], high-temperature superconductivity [19–22], and low-density superhardness [23–25]. The extra couplings between the two types of interactions at different length scales may provide opportunities to generate unexpected emergent effects [9,10].

In this paper, we demonstrate that two intriguing cluster- and energy-separated extreme states exist in a synthesized fulleride solid $[Co_6Se_8(PEt_3)_6][C_{60}]_2$ [26], which is composed of hexagonal C_{60} layers and ligand protected metal clusters $Co_6Se_8(PEt_3)_6$. Based on first-principles calculations, we reveal that the emergent superatomic Dirac state and the flat band with extreme effective mass (zero vs. infinity) are formed by the constituent C_{60} layers and $Co_6Se_8(PEt_3)_6$ clusters, respectively. Furthermore, the physics and device applications of such extreme frontier states are discussed in detail.

As well-known examples of the superatomic materials, C_{60}-based solids, e.g., fullerites [27,28] and fullerides [21,22,29,30], have been widely synthesized, benefited by the unique hollow spherical structure and very high stability of C_{60}. Assembling of C_{60} is usually driven by several ways [9,10]: (i) van der Waals (vdW) interactions, (ii) covalent bonding using photopolymerization, (iii) high-pressure and high-temperature synthesis, and (vi) using other atoms, clusters, or organic molecules as linkers. To imitate the atomic solids with ionic bonding, Roy *et al.* [26] proposed a distinctive strategy for synthesizing stable assembly by taking the electron-poor and -rich clusters with comparable size and shape as building blocks. Following this idea, they demonstrated that the metal chalcogenide cluster $Co_6Se_8(PEt_3)_6$ (**1**) and C_{60} can be assembled into an ordered binary solid **1** $\cdot$ 2C_{60} with CdI_2-type structure. The corresponding superatomic character and the resemblance between **1** $\cdot$ 2C_{60} and the atomic solid in ionic bonding were subsequently confirmed by theoretical calculations [31].

The atomic structure of **1** $\cdot$ 2C_{60} crystal is illustrated in Fig. 1, which is composed of C_{60} layers separated by **1** clusters and holds P$\bar{3}$ (No.147) symmetry. If every C_{60} cluster is regarded as a giant atom, the C_{60}-based layer resembles the honeycomb lattice of graphene (view along the [001] direction) with a low-buckling height of 3.94 Å. The centroid-to-centroid distance of 9.91 Å and the shortest nonbonded C-C distance of 3.54 Å between intralayer adjacent C_{60} cages are very close to those of interlayer C_{60} in face-centered cubic

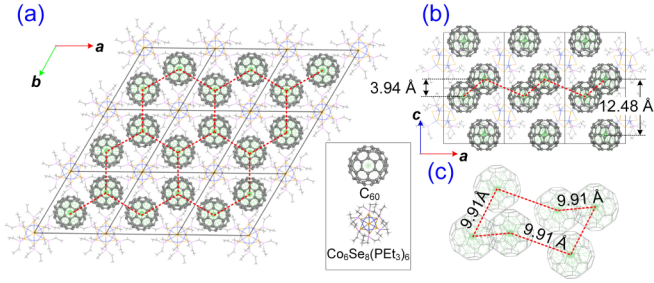*zfliu@imu.edu.cn
†zhaojj@dlut.edu.cn

FIG. 1. Crystal structure for the $3 \times 3 \times 2$ supercell of superatomic solid $\mathbf{1} \cdot 2C_{60}$: (a) the top and (b) side views based on the c axis, and (c) the perspective structure for a buckled C_{60}s hexagon in $\mathbf{1} \cdot 2C_{60}$.

(fcc) fullerite [32]. Thus, the intralayer C_{60}-C_{60} interactions should belong to the vdW type (Fig. S1(a) in the Supplemental Material [33]). However, the interaction between C_{60} buckyballs in different layers is negligible since the large intercluster distance of 12.48 Å [Fig. 1(b)] is beyond the scope of C_{60}-C_{60} interaction (Fig. S1(b) in the Supplemental Material [33]). Therefore, the graphenelike hexagonal C_{60} layers in $\mathbf{1} \cdot 2C_{60}$, termed as *fullerenenes*, can be considered mutually isolated quasi-two-dimensional (2D) superatomic systems supported by $\mathbf{1}$ clusters with ionic interaction (Fig. S2 in the Supplemental Material [33]). Inspired by these unique structural features, we carry out a systematic investigation for the electronic structure of $\mathbf{1} \cdot 2C_{60}$, aiming to unveil the unprecedented superatomic emergent states and their possible applications.

II. COMPUTATIONAL METHODS

The electronic structure calculations of the $\mathbf{1} \cdot 2C_{60}$ solid were performed using density functional theory (DFT) [33], as implemented in VASP [34]. Within the generalized gradient approximation parameterized by the Perdew-Burke-Ernzerhof functional [35], the projector augmented wave method [36] was adopted to describe the core-valence interactions with a 550 eV energy cutoff for the plane-wave basis. A Monkhorst-Pack $\mathbf{k}$-point mesh [37] with a uniform spacing of $2\pi \times 0.01$ Å^{-1} was used to sample the Brillouin zone. With experimental lattice constants, the atomic positions were fully relaxed with tolerances of 10^{-8} eV in total energy and 0.01 eV/Å in force, respectively. In consideration of the existence of C_{60}-C_{60} vdW interactions in the quasi-2D fullerenenes, the DFT-TS dispersion correction scheme [38] was used, the reliability of which has been proven to be valid for the studied $\mathbf{1} \cdot 2C_{60}$ (see Fig. S3 and Table S1 in the Supplemental Material [33]).

III. RESULTS AND DISCUSSION

As depicted in Fig. 2(a), one can see that $\mathbf{1} \cdot 2C_{60}$ is a semiconductor with a narrow bandgap of 58 meV rather than a graphenelike semimetal. Notably, there are two extreme electronic states around the Fermi level. One feature is the emergency of linear Dirac state at $\mathbf{k}$-points of K($\frac{1}{3}$, $\frac{1}{3}$, 0) and H($\frac{1}{3}$, $\frac{1}{3}$, $\frac{1}{2}$) in the two lowest conduction bands, which make the carriers massless. On the other hand, the top valence band
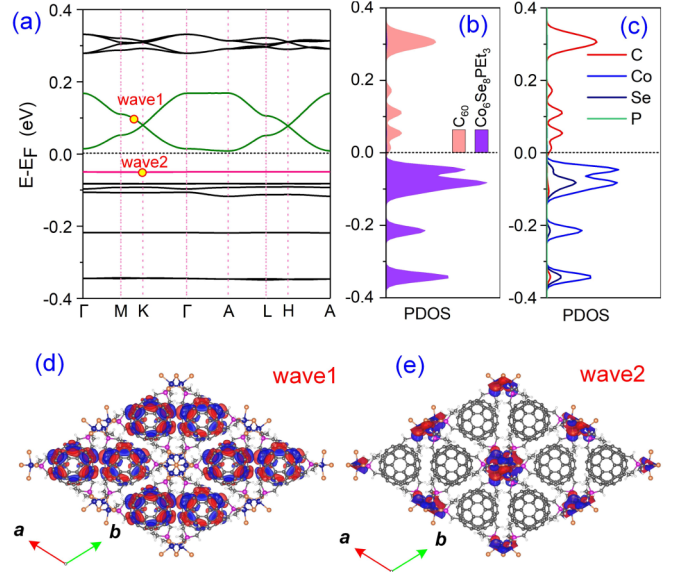

FIG. 2. (a) The electronic band structure of $\mathbf{1} \cdot 2C_{60}$; (b) clusters [i.e., C_{60} and $\mathbf{1}$ $Co_6Se_8(PEt_3)_6$], and (c) atoms (C, Co, Se, and P) projected density of states (PDOS); the visualizations of real space wave functions for (d) the linear Dirac band and (e) the flat band at two considered $\mathbf{k}$-points [see the highlighted points in (a)].

is flat without any dispersion, in which the kinetic energy of the carriers should be quenched due to their arbitrarily large effective mass. To figure out the origins of these extreme electronic states, we further calculated the projected density of states of the constituent clusters and atoms, as well as the real-space wave functions for the Dirac and flat bands. As depicted in Figs. 2(b)–2(e), the Dirac state is contributed completely by the C_{60} clusters, i.e., 2D fullerenenes, while the flat band comes from the $\mathbf{1}$ clusters; these two kinds of electronic states are well separated in both energy space and real space. Moreover, they are also extreme according to band dispersion or effective mass (zero vs infinity). In this sense, the frontier electronic states of $\mathbf{1} \cdot 2C_{60}$ can be characterized as cluster- and energy-separated extreme electronic states.

To understand the mechanism of the flat band, we consider the electron hopping Hamiltonian for a general lattice, which can be written as [39]

$$H_{\text{hop}} = \sum_{i,j,a,b} t_{ia,jb} c_{i,a}^{\dagger} c_{j,b}. \quad (1)$$

Here, i and j index $\mathbf{1}$ clusters; a and b denote different orbitals within one cluster; and $\{t\}$ are the hopping matrix elements. Using the Bloch theorem, it can also be transformed to the momentum space as

$$h_{\mathbf{k}} = \sum_{\mathbf{k},a,b} c_{\mathbf{k},a}^{\dagger} h_{ab}(\mathbf{k}) c_{\mathbf{k},b}. \quad (2)$$

Thus, the Bloch bands $\{\varepsilon_{n\mathbf{k}}\}$ can be obtained by solving the eigenvalue problem of $h(\mathbf{k})$. In an extreme case, if $t_{ia,jb}$ is equal to zero, the corresponding solution should be $\varepsilon_{n\mathbf{k}} = $ const. This means that, when the building blocks (atoms or clusters) are completely isolated without interaction, the Bloch bands should be exactly dispersionless. In the superatomic solid $\mathbf{1} \cdot 2C_{60}$, the component $\mathbf{1}$ clusters arrange in
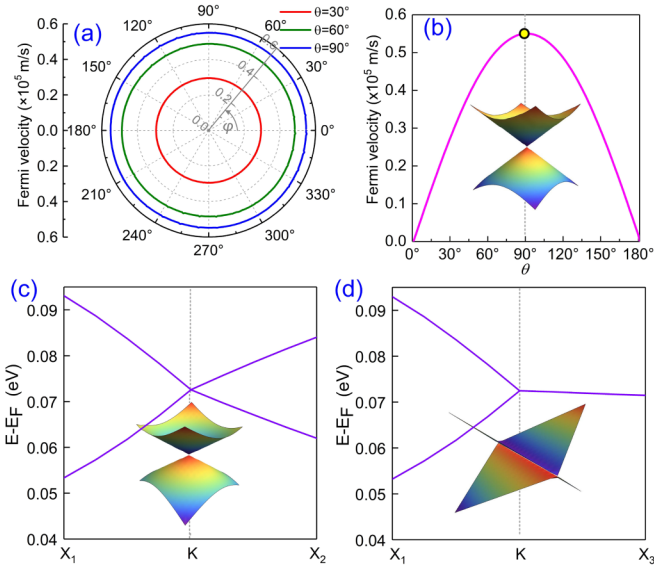
FIG. 3. The carrier velocities for the linear Dirac bands around the high-symmetry **k**-point K in different directions: (a) for a fixed θ ($30°$, $60°$, $90°$) and $\varphi = 0\text{--}360°$, (b) for any fixed φ and $\theta = 0\text{--}180°$. In the polar diagram (a), the radial direction represents the value of Fermi velocity ranged from 0 to 0.6×10^5 m/s; the angle φ is the corresponding polar angle. The inset in (b) is the three-dimensional (3D) Dirac cone for the $k_z = 0$ plane, i.e., $\theta = 90°$ and $\varphi = 0\text{--}360°$. The band structures along (c) $X_1 \rightarrow K \rightarrow X_2$ and (d) $X_1 \rightarrow K \rightarrow X_3$. The insets are the corresponding 3D band structures in the X_1-K-X_2 and X_1-K-X_3 planes.

a triangle lattice with centroid-centroid distance of 12.48 Å and nonbonded H-H spacing of 3.04 Å between two adjacent **1** clusters. As a consequence, the well-isolated **1** clusters in $\mathbf{1} \cdot 2C_{60}$ form a series of flat bands associated with the molecular orbitals of the $Co_6Se_8(PEt_3)_6$ cluster, including the top valence band shown in Fig. 2(a).

Evidently, the Dirac state is derived from the 2D substructures, fullerenenes. However, the fullerenene layers are not

completely isolated, inhabiting the three-dimensional crystalline environment. Thus, it is highly necessary to explore the feature of superatomic Dirac band dispersions along different orientations. To this end, a spherical coordinate system was constructed in the defined k'_x-k'_y-k'_z reciprocal space system centered by the high-symmetry **k**-point K (Fig. S4 in the Supplemental Material [33]), where k'_y is along the path of $K \rightarrow M$ and k'_z along $K \rightarrow H$. Then the band structures along 1440 uniformly sampled **k**-paths [denoted by (θ, φ)] were calculated. Because linear dispersion is found in all considered **k**-paths, we further evaluated the corresponding Fermi velocities $v_F(\theta, \varphi)$ of carriers using the following equation:

$$v_F(\mathbf{k}) = \frac{1}{\hbar} \frac{\partial E(\mathbf{k})}{\partial \mathbf{k}}. \tag{3}$$

The results show that: (i) when θ is fixed (e.g., $\theta = 90°, 60°$, or $30°$), v_F is independent of φ [Fig. 3(a)]; (ii) for any fixed φ, the carrier velocity strongly depends on θ, varying from 0 to the largest value of 0.551×10^5 m/s with θ increasing from 0 to $90°$ [Figs. 3(b)–3(d)]. For the $k_z = 0$ plane (i.e., $\theta = 90°$, corresponding to the lattice plane parallel to the fullerenenes), the Dirac state exhibits isotropic feature, forming a graphenelike Dirac cone [see inset of Fig. 3(b)]. Owing to the separation between different fullerenenes in the [001] direction, the band dispersions are quenched, forming localized flat-bands along the $K \rightarrow H$ path [i.e., $\theta = 0$, see Fig. 3(d)]. These results indicate that the fullerenene-formed superatomic Dirac state in $\mathbf{1} \cdot 2C_{60}$ is quasi-2D.

To gain more insights into the Dirac physics of superatoms, we constructed a two-band tight-binding (TB) model for the graphenelike superatomic lattice (Fig. S5 in the Supplemental Material [33]). By considering the nearest-neighbor interaction only, the TB effective Hamiltonian can be simplified as

$$H = \begin{bmatrix} \varepsilon & h_{12} \\ c.c & \varepsilon \end{bmatrix}. \tag{4}$$

Thereinto,

$$h_{12} = t\left(e^{i\mathbf{k}\boldsymbol{\delta}_1} + e^{i\mathbf{k}\boldsymbol{\delta}_2} + e^{i\mathbf{k}\boldsymbol{\delta}_3}\right) = t\left\{\exp\left[\frac{1}{2}i(k'_x - k'_y)r_0\right] + 2\exp\left[-\frac{1}{4}i(k'_x - k'_y)r_0\right]\cos\left[\frac{3}{4}r_0(k'_x + k'_y)\right]\right\}. \tag{5}$$

Here, $\boldsymbol{\delta}_j (j = 1, 2, 3)$ are the vectors that connect the center of a C_{60} buckyball to those of its three nearest neighbors (Fig. S5(a) in the Supplemental Material [33]), (k'_x, k'_y) are the coordinates of the $\mathbf{b}_1$-O-$\mathbf{b}_2$ system in the reciprocal space (Fig. S5(b) in the Supplemental Material [33]), r_0 (≈ 9.91 Å)

is the intercentroid distance between C_{60} clusters, t is the nearest neighbor hopping integral, and ε is the onsite energy. By solving the characteristic equation, the eigenvalues can be obtained as

$$E(\mathbf{k}) = \varepsilon \pm t\sqrt{3 + 2\cos\left(\frac{3}{2}r_0 k'_x\right) + 2\cos\left(\frac{3}{2}r_0 k'_y\right) + 2\cos\left[\frac{3}{2}r_0(k'_x + k'_y)\right]}. \tag{6}$$

Along the **k**-path of $M(\frac{2\pi}{3r_0}, 0, 0) \rightarrow K(\frac{4\pi}{9r_0}, \frac{4\pi}{9r_0}, 0) \rightarrow \Gamma(0, 0, 0)$, we fitted the DFT bands using Eq. (6). The obtained hopping parameter is 0.024 eV, which is much

smaller than that of graphene ($t \approx 2.8$ eV) [40] as the C_{60}-C_{60} vdW interaction in the fullerenene is greatly weaker than the C-C covalent bonding in graphene. The fitted onsite energy
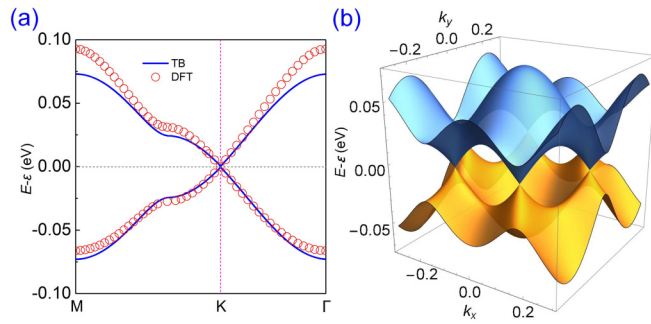
FIG. 4. (a) Comparison of electronic band structures from density functional theory (DFT; red hollow circle) and the tight-binding (TB; blue line) model. (b) Dirac cone formed by the two bands of the TB model in the k_x-k_y plane around the Dirac point.

ε is 0.08 eV, which indeed gives the position of the Dirac point deviated from the Fermi level. As displayed in Fig. 4(a), our two-band TB model can not only describe the linear Dirac bands of quasi-2D fullerenene in $1 \cdot 2C_{60}$ well but also reproduce the feature of the isotropic Dirac cone in the k_x-k_y plane [Fig. 4(b)]. The corresponding carrier velocity of 0.548×10^5 m/s ($v_F = 3r_0t/2\hbar$) is also consistent with the DFT value (0.551×10^5 m/s).

As is known, the gapless semimetallic state of conventional Dirac semimetals is usually in conflict with the bandgap prerequisite for microelectronic devices, like field effect transistor (FET) [41,42]. To realize the device applications, many strategies have been introduced to open a bandgap in the Dirac semimetals (e.g., graphene and silicene), including substrate interaction [42,43], carving a 2D sheet into a nanoribbon [44,45], applying vertical electronic field [41], and hydrogenation or chlorination [46–48]. However, when the Dirac state is broken, the fascinating properties derived from the massless linear dispersion would disappear, and the host material would be transformed into an ordinary semiconductor. In this sense, there is an irreconcilable contradiction between the gapless Dirac state and the bandgap requirement for FET applications. Intriguingly, $1 \cdot 2C_{60}$ may be able to overcome such a contradiction due to the following two features: (i) it is an intrinsic semiconductor satisfying the bandgap requirement; (ii) it possesses a quasi-2D Dirac state in the low-energy conduction bands. Hence, without opening the Dirac point, the superatomic semiconductor can realize the desirable device application with massless Dirac fermion transport by tuning the position of the Fermi level via carrier doping (see Fig. S6 in the Supplemental Material [33]) or gate voltage [49].

Stimulated by the boom of graphene [50], more and more 2D Dirac semimetals [51–57] have been proposed. In most of them, however, the identified Dirac states are based on the freestanding structures. In practical device architecture, the 2D films usually need to be placed on a substrate, which may inevitably disturb the desired Dirac state [43]. Unlike the conventional 2D Dirac semimetals, the quasi-2D fullerenenes in $1 \cdot 2C_{60}$ are naturally supported by the ionic interaction between the building blocks, i.e., $Co_6Se_8(PEt_3)_6$ and C_{60}, which not only ensures the structural stability but also endows a clean Dirac state near the Fermi level. In this regard,
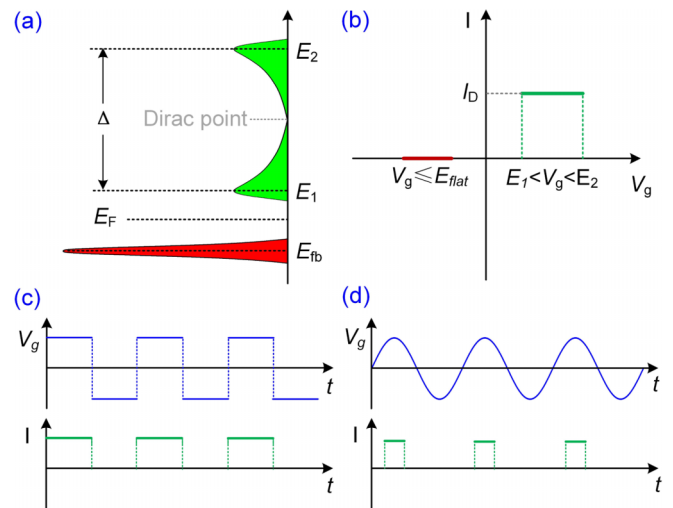

FIG. 5. (a) Schematic density of states for the two extreme states beside the Fermi level E_F. The relationships between electronic current (I) and gate voltage (V_g) in cases of (b) static V_g and oscillated V_g as time (t) goes on in (c) rectangular and (d) sinusoidal forms.

the fullerenene with natural support should be an intriguing quasi-2D Dirac material. Of course, its practical application in electronic devices needs appropriate carrier doping (see Fig. S6 in the Supplemental Material [33]) or gate voltage regulation because its Dirac state resides in the conducting bands.

Finally, physics phenomena and device applications are also expected from the coexistence of the cluster- and energy-separated extreme electronic states. In field-effect devices, a gate voltage (V_g) can be applied to the semiconductor to tune the position of the Fermi level. As the Fermi level is shifted up into the $\triangle$ energy window of $1 \cdot 2C_{60}$ [Fig. 5(a)], the massless Dirac fermions become the dominant carriers and give rise to ultrafast Dirac current, I_D in Fig. 5(b). In contrast, when the Fermi level is moved to the position of the flat band, the ultraheavy carriers will be highly localized, and the corresponding electric current should be zero. Therefore, a kind of Dirac field-effect device can be constructed on the basis of the unique cluster- and energy-separated extreme electronic states, which features the one-way ultrafast Dirac carrier transport. Moreover, when an oscillated gate voltage in rectangular or sinusoidal pulses is applied, the output current should be one-way Dirac transport with the same frequency as the applied gate voltage, acting as a Dirac field-effect rectifier [see Figs. 5(c) and 5(d)].

Before closing, the following two remarks should be emphasized. (i) The coexistence of Dirac and flat bands has been discovered in some atomic materials, such as kagome crystals [39,58–60], 2D hexagonal covalent organic frameworks [61], and twisted sandwiched graphene [62]. However, the formation mechanisms of their extreme states are completely different from that in the superatomic solid $1 \cdot 2C_{60}$. (ii) The extreme states proposed in this paper are unique (separated in both real space and energy scale, residing on the upper and lower sides of the Fermi level, and being a semiconductor) because of the emergent effect of clusters, which results in

distinctive applications in microelectronics, such as a Dirac field-effect device/rectifier.

IV. CONCLUSIONS

In summary, our first-principles calculations and theoretical analyses have identified two intriguing superatomic emergent states, i.e., cluster- and energy-separated extreme electronic states, in the synthesized $1 \cdot 2C_{60}$ solid. In the top valence band, the component **1** clusters form a flat band because of the isolated cluster environment, while in the lowest conduction bands, a so-called quasi-2D superatomic Dirac state is formed by the honeycomb C_{60} layers, fullerenenes, originated from the combination of vdW and ionic interactions. Unlike the case of conventional Dirac semimetals, the superatomic Dirac state exists in a semiconductor, which might resolve the longstanding contradiction between the gapless Dirac state and the bandgap requirement for microelectronic devices. Remarkably, we show that the emergent extreme electronic states can be utilized to build a kind of device featuring one-way Dirac carrier transport, i.e., a Dirac field-effect device/rectifier. In this paper, we pave an avenue toward quantum states based on the emergent phenomena of superatomic materials.

ACKNOWLEDGMENTS

[1] D. E. Bergeron, A. W. Castleman, T. Morisato, and S. N. Khanna, Formation of $Al_{13}I^-$: Evidence for the superhalogen character of Al_{13}, Science **304**, 84 (2004).

[2] D. E. Bergeron, P. J. Roach, A. W. Castleman, N. O. Jones, and S. N. Khanna, Al cluster superatoms as halogens in polyhalides and as alkaline earths in iodide salts, Science **307**, 231 (2005).

[3] J. U. Reveles, S. N. Khanna, P. J. Roach, and A. W. Castleman, Multiple valence superatoms, Proc. Natl. Acad. Sci. USA **103**, 18405 (2006).

[4] J. U. Reveles, P. A. Clayborne, A. C. Reber, S. N. Khanna, K. Pradhan, P. Sen, and M. R. Pederson, Designer magnetic superatoms, Nat. Chem. **1**, 310 (2009).

[5] X. Zhang, Y. Wang, H. Wang, A. Lim, G. Gantefoer, K. H. Bowen, J. U. Reveles, and S. N. Khanna, On the existence of designer magnetic superatoms, J. Am. Chem. Soc. **135**, 4856 (2013).

[6] Z. Liu, X. Liu, and J. Zhao, Design of superhalogens using a core-shell structure model, Nanoscale **9**, 18781 (2017).

[7] J. Zhao, Q. Du, S. Zhou, and V. Kumar, Endohedrally doped cage clusters, Chem. Rev. **120**, 9021 (2020).

[8] P. Jena and Q. Sun, Super atomic clusters: Design rules and potential for building blocks of materials, Chem. Rev. **118**, 5755 (2018).

[9] E. A. Doud, A. Voevodin, T. J. Hochuli, A. M. Champsaur, C. Nuckolls, and X. Roy, Superatoms in materials science, Nat. Rev. Mater. **5**, 371 (2020).

[10] S. A. Claridge, A. W. Castleman, S. N. Khanna, C. B. Murray, A. Sen, and P. S. Weiss, Cluster-assembled materials, ACS Nano **3**, 244 (2009).

[11] S. N. Khanna and P. Jena, Assembling Crystals from Clusters, Phys. Rev. Lett. **69**, 1664 (1992).

[12] M. Qian, A. C. Reber, A. Ugrinov, N. K. Chaki, S. Mandal, H. M. Saavedra, S. N. Khanna, A. Sen, and P. S. Weiss, Cluster-assembled materials: Toward nanomaterials with precise control over properties, ACS Nano **4**, 235 (2010).

[13] Q. Du, Z. Wang, S. Zhou, J. Zhao, and V. Kumar, Searching for cluster lego blocks for three-dimensional and two-dimensional assemblies, Phys. Rev. Materials **5**, 066001 (2021).

[14] Z. Liu, X. Wang, J. Cai, G. Liu, P. Zhou, K. Wang, and H. Zhu, From the ZnO hollow cage clusters to ZnO nanoporous phases: A first-principles bottom-up prediction, J. Phys. Chem. C **117**, 17633 (2013).

[15] Z. Liu, X. Wang, J. Cai, and H. Zhu, Room-temperature ordered spin structures in cluster-assembled single $V@Si_{12}$ sheets, J. Phys. Chem. C **119**, 1517 (2015).

[16] S. Mandal, A. C. Reber, M. Qian, R. Liu, H. M. Saavedra, S. Sen, P. S. Weiss, S. N. Khanna, and A. Sen, Synthesis, structure and band gap energy of covalently linked cluster-assembled materials, Dalton Trans. **41**, 12365 (2012).

[17] N. K. Chaki, S. Mandal, A. C. Reber, M. Qian, H. M. Saavedra, P. S. Weiss, S. N. Khanna, and A. Sen, Controlling band gap energies in cluster-assembled ionic solids through internal electric fields, ACS Nano **4**, 5813 (2010).

[18] S. Mandal, A. C. Reber, M. Qian, P. S. Weiss, S. N. Khanna, and A. Sen, Controlling the band gap energy of cluster-assembled materials, Acc. Chem. Res. **46**, 2385 (2013).

[19] M. Capone, M. Fabrizio, C. Castellani, and E. Tosatti, Colloquium: Modeling the unconventional superconducting properties of expanded A_3C_{60} fullerides, Rev. Mod. Phys. **81**, 943 (2009).

[20] V. A. Kulbachinskii, Y. V. Zubavichus, R. D. Svetogorov, N. S. Ezhikov, R. A. Lunin, and B. M. Bulychev, Preparation and superconducting behavior of triammonium fulleride, Carbon **182**, 51 (2021).

[21] A. F. Hebard, M. J. Rosseinsky, R. C. Haddon, D. W. Murphy, S. H. Glarum, T. T. M. Palstra, A. P. Ramirez, and A. R. Kortan, Superconductivity at 18 K in potassium-doped C_{60}, Nature (London) **350**, 600 (1991).

[22] K. Holczer, O. Klein, S.-M. Huang, R. B. Kaner, K.-J. Fu, R. L. Whetten, and F. Diederich, Alkali-fulleride superconductors: Synthesis, composition, and diamagnetic shielding, Science **252**, 1154 (1991).

[23] E. Burgos, E. Halac, R. Weht, H. Bonadeo, E. Artacho, and P. Ordejon, New Superhard Phases for Three-Dimensional C_{60}-Based Fullerites, Phys. Rev. Lett. **85**, 2328 (2000).

[24] A.-H. Cao, W.-J. Zhao, and L.-H. Gan, Fullerene-based low-density superhard materials with tunable bandgaps, Chem. Phys. Lett. **701**, 131 (2018).

[25] Y. Guo, L. Cui, D. Zhao, T. Song, X. Cui, and Z. Liu, T-C_{56}: A low-density transparent superhard carbon allotrope assembled from C_{16} cage-like cluster, J. Phys.: Condens. Matter **32**, 165701 (2020).

[26] X. Roy, C.-H. Lee, A. C. Crowther, C. L. Schenck, T. Besara, R. A. Lalancette, T. Siegrist, P. W. Stephens, L. E. Brus, P. Kim, M. L. Steigerwald, and C. Nuckolls, Nanoscale atoms in solid-state chemistry, Science **341**, 157 (2013).

[27] M. Núñez-Regueiro, L. Marques, J. L. Hodeau, O. Bethoux, and M. Perroux, Polymerized Fullerite Structures, Phys. Rev. Lett. **74**, 278 (1995).

[28] W. Krätschmer, L. D. Lamb, K. Fostiropoulos, and D. R. Huffman, Solid C_{60}: A new form of carbon, Nature (London) **347**, 354 (1990).

[29] R. M. Fleming, M. J. Rosseinsky, A. P. Ramirez, D. W. Murphy, J. C. Tully, R. C. Haddon, T. Siegrist, R. Tycko, S. H. Glarum, P. Marsh, G. Dabbagh, S. M. Zahurak, A. V. Makhija, and C. Hampton, Preparation and structure of the alkali-metal fulleride A_4C_{60}, Nature (London) **352**, 701 (1991).

[30] J. Arvanitidis, K. Papagelis, S. Margadonna, K. Prassides, and A. N. Fitch, Temperature-induced valence transition and associated lattice collapse in samarium fulleride, Nature (London) **425**, 599 (2003).

[31] L. Hammerschmidt, J. Schacht, and N. Gaston, First-principles calculations of the electronic structure and bonding in metal cluster-fullerene materials considered within the superatomic framework, Phys. Chem. Chem. Phys. **18**, 32541 (2016).

[32] Y. Iwasa, T. Arima, R. M. Fleming, T. Siegrist, O. Zhou, R. C. Haddon, L. J. Rothberg, K. B. Lyons, H. L. Carter, Jr., A. F. Hebard, R. Tycko, G. Dabbagh, J. J. Krajewski, G. A. Thomas, and T. Yagi, New phases of C_{60} synthesized at high pressure, Science **264**, 1570 (1994).

[33] See Supplemental Material at http://link.aps.org/supplemental/10.1103/PhysRevB.105.115132 for C_{60}-C_{60} interaction energy as a function of centroid distance (Fig. S1), deformation charge density of $1 \cdot 2C_{60}$ with respect to its components (Fig. S2), energy-volume curves from different methods (Fig. S3), Brillouin zone of $1 \cdot 2C_{60}$ and the defined spherical coordinate system (Fig. S4), the superatomic lattice of a 2D fullerenene and its Brillouin zone (Fig. S5), the electronic properties of $1 \cdot 2C_{60}$ under electrons doping (Fig. S6), and the related physics parameters obtained from different methods (Table S1), which includes Refs. [63–69].

[34] G. Kresse and J. Furthmuller, Efficient iterative schemes for *ab initio* total-energy calculations using a plane-wave basis set, Phys. Rev. B **54**, 11169 (1996).

[35] J. P. Perdew, K. Burke, and M. Ernzerhof, Generalized Gradient Approximation Made Simple, Phys. Rev. Lett. **77**, 3865 (1996).

[36] G. Kresse and D. Joubert, From ultrasoft pseudopotentials to the projector augmented-wave method, Phys. Rev. B **59**, 1758 (1999).

[37] H. J. Monkhorst and J. D. Pack, Special points for Brillouin-zone integrations, Phys. Rev. B **13**, 5188 (1976).

[38] A. Tkatchenko and M. Scheffler, Accurate Molecular van der Waals Interactions from Ground-State Electron Density and Free-Atom Reference Data, Phys. Rev. Lett. **102**, 073005 (2009).

[39] Z. Liu, F. Liu, and Y.-S. Wu, Exotic electronic states in the world of flat bands: from theory to material, Chin. Phys. B **23**, 077308 (2014).

[40] A. H. Castro Neto, F. Guinea, N. M. R. Peres, K. S. Novoselov, and A. K. Geim, The electronic properties of graphene, Rev. Mod. Phys. **81**, 109 (2009).

[41] Z. Ni, Q. Liu, K. Tang, J. Zheng, J. Zhou, R. Qin, Z. Gao, D. Yu, and J. Lu, Tunable bandgap in silicene and germanene, Nano Lett. **12**, 113 (2012).

[42] K. Novoselov, Mind the gap, Nat. Mater. **6**, 720 (2007).

[43] S. Y. Zhou, G. H. Gweon, A. V. Fedorov, P. N. First, W. A. de Heer, D. H. Lee, F. Guinea, A. H. Castro Neto, and A. Lanzara, Substrate-induced bandgap opening in epitaxial graphene, Nat. Mater. **6**, 770 (2007).

[44] Y. W. Son, M. L. Cohen, and S. G. Louie, Energy Gaps in Graphene Nanoribbons, Phys. Rev. Lett. **97**, 216803 (2006).

[45] M. Y. Han, B. Ozyilmaz, Y. Zhang, and P. Kim, Energy Band-Gap Engineering of Graphene Nanoribbons, Phys. Rev. Lett. **98**, 206805 (2007).

[46] J. O. Sofo, A. S. Chaudhari, and G. D. Barber, Graphane: A two-dimensional hydrocarbon, Phys. Rev. B **75**, 153401 (2007).

[47] D. C. Elias, R. R. Nair, T. M. G. Mohiuddin, S. V. Morozov, P. Blake, M. P. Halsall, A. C. Ferrari, D. W. Boukhvalov, M. I. Katsnelson, A. K. Geim, and K. S. Novoselov, Control of graphene's properties by reversible hydrogenation: Evidence for graphane, Science **323**, 610 (2009).

[48] J. T. Robinson, J. S. Burgess, C. E. Junkermeier, S. C. Badescu, T. L. Reinecke, F. K. Perkins, M. K. Zalalutdniov, J. W. Baldwin, J. C. Culbertson, P. E. Sheehan, and E. S. Snow, Properties of fluorinated graphene films, Nano Lett. **10**, 3001 (2010).

[49] X. Li, X. Wu, Z. Li, J. Yang, and J. G. Hou, Bipolar magnetic semiconductors: a new class of spintronics materials, Nanoscale **4**, 5680 (2012).

[50] K. S. Novoselov, A. K. Geim, S. V. Morozov, D. Jiang, Y. Zhang, S. V. Dubonos, I. V. Grigorieva, and A. A. Firsov, Electric field effect in atomically thin carbon films, Science **306**, 666 (2004).

[51] D. Malko, C. Neiss, F. Vines, and A. Gorling, Competition for Graphene: Graphynes with Direction-Dependent Dirac Cones, Phys. Rev. Lett. **108**, 086804 (2012).

[52] X.-F. Zhou, X. Dong, A. R. Oganov, Q. Zhu, Y. Tian, and H.-T. Wang, Semimetallic Two-Dimensional Boron Allotrope with Massless Dirac Fermions, Phys. Rev. Lett. **112**, 085502 (2014).

[53] G. Liu, S. B. Liu, B. Xu, C. Y. Ouyang, H. Y. Song, S. Guan, and S. A. Yang, Multiple Dirac points and hydrogenation-induced magnetism of germanene layer on Al (111) surface, J. Phys. Chem. Lett. **6**, 4936 (2015).

[54] J. Wang, S. Deng, Z. Liu, and Z. Liu, The rare two-dimensional materials with dirac cones, Natl. Sci. Rev. **2**, 22 (2015).

[55] Z. Wang, X. F. Zhou, X. Zhang, Q. Zhu, H. Dong, M. Zhao, and A. R. Oganov, Phagraphene: a low-energy graphene allotrope composed of 5-6-7 carbon rings with distorted Dirac cones, Nano Lett. **15**, 6182 (2015).

[56] S. M. Young and C. L. Kane, Dirac Semimetals in Two Dimensions, Phys. Rev. Lett. **115**, 126803 (2015).

[57] Z. F. Liu, W. X. Feng, H. L. Xin, Y. L. Gao, P. F. Liu, Y. G. Yao, H. M. Weng, and J. J. Zhao, Two-dimensional spin-valley-

coupled Dirac semimetals in functionalized SbAs monolayers, Mater. Horiz. **6**, 781 (2019).

[58] C. Zhong, Y. Xie, Y. Chen, and S. Zhang, Coexistence of flat bands and dirac bands in a carbon-kagome-lattice family, Carbon **99**, 65 (2016).

[59] M. Kang, L. Ye, S. Fang, J. S. You, A. Levitan, M. Han, J. I. Facio, C. Jozwiak, A. Bostwick, E. Rotenberg, M. K. Chan, R. D. McDonald, D. Graf, K. Kaznatcheev, E. Vescovo, D. C. Bell, E. Kaxiras, J. van den Brink, M. Richter, M. Prasad Ghimire *et al.*, Dirac fermions and flat bands in the ideal kagome metal FeSn, Nat. Mater. **19**, 163 (2020).

[60] M. Li, Q. Wang, G. Wang, Z. Yuan, W. Song, R. Lou, Z. Liu, Y. Huang, Z. Liu, H. Lei, Z. Yin, and S. Wang, Dirac cone, flat band and saddle point in kagome magnet YMn_6Sn_6, Nat. Commun. **12**, 3129 (2021).

[61] X. Ni, H. Li, F. Liu, and J. L. Bredas, Engineering of flat bands and dirac bands in two-dimensional covalent organic frameworks (COFs): Relationships among molecular orbital symmetry, lattice symmetry, and electronic-structure characteristics, Mater. Horiz. **9**, 88 (2022).

[62] S. Carr, C. Li, Z. Zhu, E. Kaxiras, S. Sachdev, and A. Kruchkov, Ultraheavy and ultrarelativistic Dirac quasiparticles in sandwiched graphenes, Nano Lett. **20**, 3030 (2020).

[63] Y. J. Dappe, J. Ortega, and F. Flores, Intermolecular interaction in density functional theory: Application to carbon nanotubes and fullerenes, Phys. Rev. B **79**, 165409 (2009).

[64] J. P. K. Doye, D. J. Wales, W. Branz, and F. Calvo, Modeling the structure of clusters of C_{60} molecules, Phys. Rev. B **64**, 235409 (2001).

[65] L. A. Girifalco, Molecular properties of fullerene in the gas and solid phases, J. Phys. Chem. **96**, 858 (1992).

[66] F. I. K. Momma, VESTA 3 for three-dimensional visualization of crystal, volumetric and morphology data, J. Appl. Cryst. **44**, 1272 (2011).

[67] S. Grimme, J. Antony, S. Ehrlich, and H. Krieg, A consistent and accurate *ab initio* parametrization of density functional dispersion correction (DFT-D) for the 94 elements H-Pu, J. Chem. Phys. **132**, 154104 (2010).

[68] S. Grimme, S. Ehrlich, and L. Goerigk, Effect of the damping function in dispersion corrected density functional theory, J. Comput. Chem. **32**, 1456 (2011).

[69] Y. Hinuma, G. Pizzi, Y. Kumagai, F. Oba, and I. Tanaka, Band structure diagram paths based on crystallography, Comput. Mater. Sci. **128**, 140 (2017).